Multiple scale analysis of energy harvesting in aeroelastic system in flutter condition

Ana Carolina Godoy Amaral[1], Marcos Silveira[1]

[1]*Sao Paulo State University (UNESP), School of Engineering*
Av. Eng. Luiz Edmundo C. Coube 14-01, Vargem Limpa, 17033-360, São Paulo/Bauru , Brazil
ana.carolina@unesp.br, marcos.silveira@unesp.br

Abstract. The ever increasing need for efficient, environmental-friendly and sustainable energy sources has propelled the study of energy harvesting and its applications in many fields of engineering in the last decade. Nonlinear aspects of energy harvesting have been extensively investigated for two main reasons: improve the accuracy of the mathematical models of systems that inherently present nonlinear behaviour, and to intentionally introduce nonlinear behaviour to the system in order to improve the harvesting performance. Electrical nonlinear aspects can have large influence on the harvesting device. Investigations of the effect of quadratic nonlinear piezoelectrical coupling showed that the amount of harvested power can be significantly influenced. In this paper, we show the contributions of cubic nonlinear stiffness on the dynamic behaviour of an aeroelastic energy harvesting system. Analytically, each case is analysed using the method of multiple scales. The first case is a linear system with finite degrees of freedom, the second case evaluates forced oscillations of system having cubic nonlinearity. We relate natural frequencies present in the system and target energy transfers (TET). TET uses non-linear modes and internal resonance to transfer vibration energy, passively. Numerically, the response is calculated using a 4th order Runge-Kutta method. The results for the analysed system indicate that cubic nonlinear stiffness has more influence in increasing flutter speed than increasing electrical power.

Keywords: Nonlinear, energy harvesting, flutter

1 Introduction

Energy harvesting is a technology that has been explored by researchers as an alternative to nonrenewable energy resources in recent years [1], because it is a promising technology to produce sustainable energy sources, replacing fossil fuel. There are many ways to harvest energy: electromagnetic, piezoelectric, thermoelectric, pyroelectric, photovoltaic and solar heat collector [2, 3]. Energy harvesters are designed to extract energy from ambient mechanical vibration and transfer it to electrical devices [4]. Energy harvesting sources are very varied, such as vibrational sources, RF sources, thermal sources, and energy transducers can also be very varied, such as techniques for capturing energy and its storage and distribution. It is important to extract the maximum output power to make this technology more viable. One way to maximize energy harvesting power output is to choose the right type of piezoelectric and the right combination of parameters [5]. But harvester performance is still an issue. The study of [6] discusses the work of a piezoelectric harvester, in which efficiency is mainly related to the electromechanical coupling effect, damping effect, excitation frequency and electric charge. Therefore, there is no formula to maximize the output power, each piezoelectric energy harvest has its own performance, due to its parameters.

One of the many fields of study in which energy harvesting can be applied is in aeronautics. It has many applications, such as generating low power electricity in various applications, ranging from aircraft and helicopters to civil structures in high wind areas [7]. Aeroelasticity is a science that studies the behaviour and mechanical properties of an elastic section or structure in interaction with air [8]. Flutter is a very important topic in aeroelasticity, the flutter phenomenon occurs when an aircraft component presents a divergent oscillatory self-sustained behaviour at a certain speed. It is an undesirable phenomenon in aircraft, as it can cause structural damage due to aeroelastic instability [9]. But this oscillatory movement, caused by the phenomenon of vibration, is an inter-

esting source of research and study for energy extraction. Besides that, one benefit of using energy harvesting in combination with vibration is that it decreases the flutter speed [10], this means that flutter speed can be increased, which can be an interesting topic for aeronautics. Another benefit of energy harvesting is extracting electrical energy from vibrating vibrations and directing it to the aircraft's electronic devices. The biggest question is how to improve this technology so that it can collect as much energy as possible. Nonlinear elements were studied as a way to maximize power output in the typical aeroelastic section and suppress flutter velocity. Nonlinear stiffness components were investigated on extracted energy and nonlinear aeroelastic behaviour [11]. The work of Triplett and Quinn [12] compares the use of nonlinear stiffness and nonlinear electromechanical coupling with the typical section with linear stiffness and linear electromechanical coupling, quantifying vibration speed, mechanical and electrical power. It is possible to see that the addition of nonlinear elements changes the system performance, so that the nonlinear electromechanical coupling can increase the system's output power, which allows extracting more energy. Sousa et al. [13] employs an inductor synchronized tap-changer damping (SSDI) technique, capable of dealing with the nonlinear characteristics of the electrical domain of the problem and the use of shape memory alloys (SMA) as an alternative to conventional actuators. The nonlinearity applied to the system, by the SMA and SSDI together, results in a better aeroelastic behaviour, for a speed range 25 % greater than in a linear system..

Multiple scales is an analytical method to provide an approximate expression of the response of a system. These methods work for small periodic finite movements in the vicinity of a center [14]. One of the advantages of this method is that it allows solving equations in the presence of damping and nonlinearity. The response of nonlinear dynamics of harvesters are studied using the multiple scale method [15, 16].

2 Mathematical model

In this section, the model and the dynamical equations of the aeroelastic typical section are described. Also, the mathematical model for aerodynamic loads is presented.

Figure 1 shows the model of the aeroelastic typical section of a system with three degrees of freedom: two mechanical degrees of freedom, plunge (h) and pitch (α), and one electrical degree of freedom, voltage (v). The piezoelectric coupling is associated to plunge.
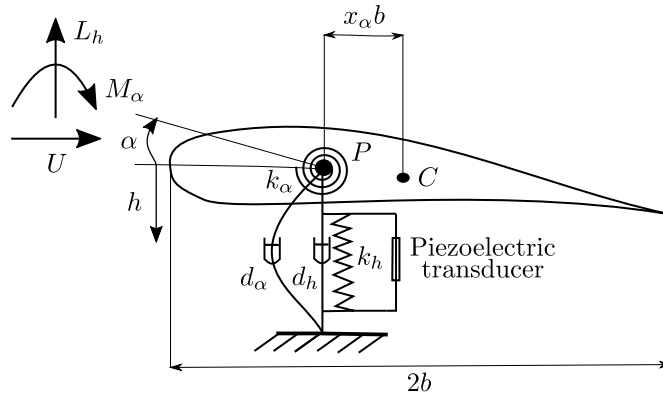
Figure 1. Aeroelastic section.

The dynamical equations, based on [17], of the system presented in fig. 1, applying the nonlinear stiffness of the cubic type associated to plunge movement and nonlinear electromechanical coupling, in dimensionless form, are given by:

$$\beta h'' + x_\alpha \alpha'' + \zeta_h h' + h + \delta h^3 - \kappa(K|h'| + 1)v = -L_h$$
$$x_\alpha h'' + r_\alpha^2 \alpha'' + \zeta_\alpha \alpha' + \gamma^2 r_\alpha^2 \alpha = M_\alpha$$
$$\eta v' + \frac{v}{\lambda} + \kappa(K|h'| + 1)h' = 0 \tag{1}$$

in which h and α are the dimensionless plunge and pitch displacements, β is the dimensionless mass ratio, ζ_h and ζ_α are the dimensionless plunge and pitch damping ratios, x_α is the dimensionless chord-wise offset of the elastic axis from the centroid, r_α is the dimensionless radius of gyration, γ is the dimensionless frequency ratio, M_α is the dimensionless aerodynamic moment, L_h is the dimensionless aerodynamic lift, κ is the dimensionless

electromechanical coupling, λ is the dimensionless load resistance, v is the dimensionless voltage electrical, η is the dimensionless equivalent capacitance, δ is the dimensionless nonlinear stiffness coefficient, K is the dimensionless nonlinear electromechanical coupling coefficient, and $'$ denotes differentiation over dimensionless time (τ).

The dimensionless terms follows the definitions used by Marqui Jr and Erturk [17], and are reproduced as follows:

$$h = \frac{\overline{h}}{b} \qquad \beta = \frac{m + m_e}{m} \qquad \zeta_h = \frac{d_h}{m\omega_h} \qquad \zeta_\alpha = \frac{d_\alpha}{mb^2\omega_h} \qquad r_\alpha = \frac{\overline{r}_\alpha}{b}$$

$$\gamma = \frac{\omega_\alpha}{\omega_h} \qquad v = \frac{\overline{v}}{v^*} \qquad \kappa = \frac{\theta v^*}{cmb\omega_h^2} \qquad \eta = \frac{C_p v^{*2}}{mb^2 c\omega_h^2} \qquad \lambda = \frac{R_l mb^2 c\omega_h^3}{v^{*2}}$$

$$L_h = \frac{L}{mb\omega_h^2} \qquad M_\alpha = \frac{M}{mb^2\omega_h^2} \qquad U = \frac{\overline{U}}{\omega_h b} \qquad \tau = \omega_h t \tag{2}$$

in which m is the typical section mass, m_e is the attachment mass, bx_α is the offset from the elastic axis to the centroid, $\overline{h}$ is the plunge displacement, d_α and d_h are the plunge and pitch damping coefficients, $\overline{r}_\alpha$ radius of gyration, c is the span length, ω_h and ω_α are the uncoupled plunge and pitch natural frequencies, $\overline{v}$ is the electrical voltage, $v^* = 1V$ is the reference voltage for normalisation, R_t is the load resistance, C_p is the piezoelectrical equivalent capacitance, θ is the piezoelectrical coupling, L is the aerodynamic lift, M is the aerodynamic moment, $\overline{U}$ is the wind speed, and t is the time.

The model for aerodynamical loads, lift (L_h) and moment (M_α), is used as presented by Dowell et al. [18] for quasi-steady incompressible flow, and reproduced here:

$$L = \rho \frac{U^2}{2} S \frac{\partial C_L}{\partial \alpha} \left[\alpha + \frac{\dot{h}}{U} \right] \qquad\qquad M = \rho \frac{U^2}{2} Se \frac{\partial C_L}{\partial \alpha} \left[\alpha + \frac{\dot{h}}{U} \right] \tag{3}$$

in which ρ is the air density, x_f is the distance from the leading edge to the neutral line, and $e = \frac{x_f}{c - 1/4}$. Note that eq. (3) is not in dimensionless form. To include this in eq. (1) one must use the dimensionless forms L_h and M_α, given by eq. (2).

3 Multiple scale analysis

In this section a multiple scale analysis of the system in 1 is developed.

By substituting L_h and M_α from eq. (2) into eq. (1), using L_h and M_α from eq. (3), the dynamical equations can be rewritten in matrix form as:

$$X'' + \hat{C}X' + \hat{K}X + \hat{G}(X) + \hat{P}v = 0$$
$$\Lambda v' + \frac{v}{\lambda} + \kappa h' = 0 \tag{4}$$

in which

$$\hat{C} = M^{-1}C \qquad \hat{K} = M^{-1}K \qquad \hat{G}(X) = M^{-1}G(X) \qquad \hat{P} = M^{-1}P \tag{5}$$

in which M is the mass matrix, K is the stiffness matrix, C is the damping matrix, G is the vector of nonlinearity, and P is the electric part matrix.

In order to apply the method of multiple scales, it is convenient to write the dynamical equations in modal form. The modal form can be used to decouple the linear terms in eq. (4). Defining the dynamic matrix of the mechanical subsystem as $A = M^{-1}K$, which has eigenvalues $\omega_{1,2}^2$ and eigenvectors $v_{1,2}$, the modal matrix is given by $\phi = [V_1 V_2]$. The modal mass, damping and stiffness matrices, force and nonlinear vectors are given by:

$$C_m = \phi^{-1}\hat{C}\phi \qquad K_m = \phi^{-1}\hat{K}\phi \qquad G_m(\eta) = \phi^{-1}\hat{G}(X)\phi \qquad P = \phi^{-1}\hat{P}\phi \tag{6}$$

in which M_m and K_m are diagonal. Using the coordinate transformation $X = \phi\eta$, the dynamical equations can be rewritten as:

$$\eta'' + C_m\eta' + K_m\eta + G_m(\eta) + P_m v = 0$$
$$v'\Lambda + \left(\frac{v}{\lambda}\right) + h'\kappa = 0 \tag{7}$$

In order to separate the eq. (7), the parameter ϵ is implemented. In this case it is used $\epsilon^2 C$ and $\epsilon^2 P$. Applying multiple scales:

$$\eta_1 = \epsilon\eta_{11}(T_0, T_2) + \epsilon^3\eta_{13}(T_0, T_2)$$
$$\eta_2 = \epsilon\eta_{21}(T_0, T_2) + \epsilon^3\eta_{23}(T_0, T_2)$$
$$v = \epsilon v_{31}(T_0, T_2) + \epsilon^3 v_{33}(T_0, T_2)$$
$$\tag{8}$$

Replacing eq. (8) in eq. (7), and equaling ϵ, ϵ^3 in both sides, it results in:

$$D_0^2\eta_{11} + \omega_1^2\eta_{11}$$
$$D_0^2\eta_{21} + \omega_2^2\eta_{21}$$
$$v_{31}/\lambda + D_0\Lambda v_{31} + D_0\eta_{11}\kappa \tag{9}$$

$$P_{e1}v_{31} + \eta_{13}\omega_1^2 - \alpha_{18}\eta_{21}^3 + \alpha_{17}\eta_{21}^3 - \alpha_{16}\eta_{11}\eta_{21}^2 + \alpha_{15}\eta_{11}\eta_{21}^2 -$$
$$\alpha_{14}\eta_{11}^2\eta_{21} + \alpha_{13}\eta_{11}^2\eta_{21} - D_0 d_2\eta_{21} + D_0^2\eta_{13} - \alpha_{12}\eta_{11}^3 + \alpha_{11}\eta_{11}^3 - D_0 d_1\eta_{11} + 2D_0 D_2\eta_{11}$$
$$-P_{e2}v_{31} + \eta_{23}\omega_2^2 + D_0^2\eta_{23} - \alpha_{26}\eta_{21}^3 + \alpha_{25}\eta_{21}^3 - \alpha_{24}\eta_{11}\eta_{21}^2 + \alpha_{23}\eta_{11}\eta_{21}^2 -$$
$$\alpha_{22}\eta_{11}^2\eta_{21} + \alpha_{21}\eta_{11}^2\eta_{21} - D_0 d_4\eta_{21} + 2D_0 D_2\eta_{21} - alpha_{20}\eta_{11}^3 + \alpha_{19}\eta_{11}^3 - D_0 d_3\eta_{11}$$
$$v_{33}/\lambda + D_0\Lambda v_{33} + D_2\Lambda v_{31} + D_0\eta_{13}\kappa + D_2\eta_{11}\kappa \tag{10}$$

The solution of eq. (9) is:

$$\eta_{11} = A_1(T_2)exp(i\omega_1 T_0) + cc$$
$$\eta_{21} = A_2(T_2)exp(i\omega_2 T_0) + cc$$
$$v_{31} = C_1 exp(-T_0/(\Lambda\lambda)) + \frac{(\overline{A_1}\kappa)}{(-(iexp(iT_0\omega_1))/(\omega_1\lambda) - \Lambda exp(iT_0\omega_1))}\frac{-(A_1\kappa exp(iT_0\omega_1))}{(\Lambda - i/(\omega_1\lambda))} \tag{11}$$

In which A_1 and A_2 are complex functions, and C_1 is a constant.
By replacing eq. (11) in eq. (10), it is possible to find secular terms.

3.1 Resonant case ($\omega_2 \approx 3\omega_1$)

The parameter σ is used to compare ω_1 and ω_2, at the resonant case $\omega_2 \approx 3\omega_1$.

$$\omega_2 = 3\omega_1 + \epsilon^2\sigma \tag{12}$$

It results in:

$$exp[i(\omega_2 - 2\omega_1)T_0] = exp(i\omega_1 T_0 + i\sigma T_2)$$
$$exp[3i\omega_1 T_0] = exp(i\omega_2 T_0 + i\sigma T_2) \tag{13}$$

The secular terms found in this resonant case are::

$$\frac{-(A_1 P_{e1}\kappa)}{(\Lambda - i/(\omega_1\lambda))} - iA_1 d_1\omega_1 + 2iA_1 D_2\omega_1 - 2A_1 A_2\overline{A_2}\alpha_{16} + 2A_1 A_2\overline{A_2}\alpha_{15} - 3A_1^2\overline{A_1}\alpha_{12} + 3A_1^2\overline{A_1}\alpha_{11} +$$

$$(\overline{A_1}^2 A_2\alpha_{13} - \overline{A_1}^2 A_2\alpha_{14})exp(iT_2\sigma) \tag{14}$$

$$-iA_2d_4\omega_2 + 2iA_2D_2\omega_2 - 3A_2^2\overline{A_2}\alpha_{26} + 3A_2^2\overline{A_2}\alpha_{25} - 2A_1\overline{A_1}A_2\alpha_{22} + 2A_1\overline{A_1}A_2\alpha_{21} +$$
$$(A_1^3\alpha_{19} - A_1^3\alpha_{20})exp(-iT_2\sigma) \tag{15}$$

It is convinient to write A in the polar form:

$$A_m = \frac{1}{2}a_m exp(i\theta_m) \tag{16}$$

in which $m = 1, 2$.

Replacing eq. (16) in eq. (14) and eq. (15), and separating the result in real and imaginary parts:

$$8\omega_1(a_1' + \frac{d_1a_1}{2} - \frac{\Lambda P_{e1}a_1\kappa\lambda^2}{2(\Lambda^2\omega_1^2\lambda^2 + 1)}) + (a_1^2a_2\alpha_{13} - a_1^2a_2\alpha_{14})\sin(\gamma) = 0$$

$$8\omega_2(a_2' + \frac{d_4a_2}{2}) + (a_1^3\alpha_{19} - a_1^3\alpha_{20})\sin(\gamma) = 0$$

$$8\omega_1(-\frac{P_{e1}a_1\kappa\omega_1^2\lambda}{2(\Lambda^2\omega_1^2\lambda^2 + 1)} + a_1\theta_1') + (a_1^2a_2\alpha_{13} - a_1^2a_2\alpha_{14})\cos(\gamma) +$$

$$a_1(-2a_2^2\alpha_{16} + 2a_2^2\alpha_{15} + 3a_1^2\alpha_{12} - 3a_1^2\alpha_{11}) = 0$$

$$8\omega_2a_2\theta_2' + (a_1^3\alpha_{19} - a_1^3\alpha_{20})\cos(\gamma) + a_2(-3a_2^2\alpha_{26} + 3a_2^2\alpha_{25} - 2a_1^2\alpha_{22} + 2a_1^2\alpha_{21}) = 0 \tag{17}$$

in which $\gamma = \theta_2 - 3\theta_1 + \sigma T_2$.

To eliminate θ_1 and θ_2 of eq. (17), it is used γ.

$$a_2\gamma' = a_2\sigma - \frac{3P_{e1}a_1a_2\kappa\omega_1\lambda}{2\Lambda^2a_1\omega_1^2\lambda^2 + 2a_1} + \frac{a_1^3\alpha_{20}\cos(\gamma)}{8\omega_2} - \frac{a_1^3\alpha_{19}\cos(\gamma)}{8\omega_2} - \frac{3a_1a_2^2\alpha_{14}\cos(\gamma)}{8\omega_1} +$$

$$\frac{3a_1a_2^2\alpha_{13}\cos(\gamma)}{8\omega_1} + \frac{3a_2^3\alpha_{26}}{8\omega_2} - \frac{3a_2^3\alpha_{25}}{8\omega_2} + \frac{a_1^2a_2\alpha_{22}}{4\omega_2} - \frac{a_1^2a_2\alpha_{21}}{4\omega_2}$$

$$-\frac{3a_2^3\alpha_{16}}{4\omega_1} + \frac{3a_2^3\alpha_{15}}{4\omega_1} + \frac{9a_1^2a_2\alpha_1 2}{8\omega_1} - \frac{9a_1^2a_2\alpha_1 2}{8\omega_1} \tag{18}$$

The equations are reduced to imaginary part of eq. (17) and eq. (18). To simplified eq. (17), the imaginary part is added, and $\sin(\gamma)$ is eliminated:

$$\frac{((4\Lambda^2a_2^2\alpha_{14} - 4\Lambda^2a_2^2\alpha_{13})d_4 + 8\Lambda^2a_2a_2'\alpha_{14} - 8\Lambda^2a_2a_2'\alpha_{13})\omega_1^2\omega_2}{((\Lambda^2\alpha_{20} - \Lambda^2\alpha_{19})\omega_1^3\lambda^2 + (\alpha_{20} - \alpha_{19})\omega_1} +$$

$$\frac{((4\Lambda^2a_1^2\alpha_{19} - 4\Lambda^2a_1^2\alpha_{20})d_1 - 8\Lambda^2a_1a_1'\alpha_{20} + 8\Lambda^2a_1a_1'\alpha_{19})\omega_1^3}{((\Lambda^2\alpha_{20} - \Lambda^2\alpha_{19})\omega_1^3\lambda^2 + (\alpha_{20} - \alpha_{19})\omega_1}$$

$$+\frac{(4\Lambda P_{e1}a_1(T_2)a_1\alpha_{20} - 4\Lambda P_{e1}a_1(T_2)a_1\alpha_{19})\kappa\omega_1^2)\lambda^2}{((\Lambda^2\alpha_{20} - \Lambda^2\alpha_{19})\omega_1^3\lambda^2 + (\alpha_{20} - \alpha_{19})\omega_1)}$$

$$+\frac{((4a_2^2\alpha_{14}4a_2^2\alpha_{13})d_4 + 8a_2a_2'\alpha_{14} - 8a_2a_2'\alpha_{13})\omega_2}{((\Lambda^2\alpha_{20} - \Lambda^2\alpha_{19})\omega_1^3\lambda^2 + (\alpha_{20} - \alpha_{19})\omega_1} +$$

$$\frac{((4a_1^2\alpha_{19} - 4a_1^2\alpha_{20})d_1 - 8a_1a_1'\alpha_{20} + 8a_1a_1'\alpha_{19})\omega_1)}{((\Lambda^2\alpha_{20} - \Lambda^2\alpha_{19})\omega_1^3\lambda^2 + (\alpha_{20} - \alpha_{19})\omega_1} = 0 \tag{19}$$

The approximated solution for the steady state motion is given by substituting eq. (20) in eq. (18) and eq. (19).

$$a_1' = a_2' = \gamma' = 0 \tag{20}$$

4 Numerical analysis

The response of the system is calculated through numerical simulation, using a 4th order Runge-Kutta method. The flutter speed was determined with an optimisation procedure based on the interval halving method (or

bissection method). In the this method, one-half of the current interval of uncertainty is discarded in every stage, until the right solution is found, for the middle point of the final interval (Rao, 2009). From a initial guess for the interval, which is taken based on the flutter speed of the linear system, and with the other parameters fixed, the optimisation procedure seeks to minimise the difference between consecutive peaks of the response in time. If the difference is zero, this gives the condition of self-sustained oscillation. Therefore, the objective function is given by:

$$f(U) = |D_f| - E \tag{21}$$

in which D_f is the difference between the penultimate amplitude peak and last amplitude peak, and E is a tolerance. Equation (21) allows the reasoning that in order for flutter to happen, the distance between the peaks must be 0. Since the equations are solved numerically, a tolerance must be considered.

The values of parameters used here are based on values from [17]: $\beta = 2.5940$, $r_\alpha = 0.5467$, $\gamma = 0.5090$, $\zeta_h = 0.0535$, $\zeta_\alpha = 0.1102$, $x_\alpha = 0.25$, $\rho = 1.2754 \text{kg/m}^3$, $b = 0.76$ m, κ varies from 2×10^{-6} to 8×10^{-6} até , $\eta = 3.66 \times 10^{-9}$, $\lambda = 0.48 \times 10^9$, $m = 92.53$ kg, $\omega_h = 50$ rad/s. The initial conditions used are $h = 0.1$, $\alpha = 0.1$, $h' = 0$ e $\alpha' = 0$ e $v = 0$.

Figure 2 shows the variation of flutter speed U^* as a function of electromechanical copuling κ. The result indicates that U^* increases with κ. Also, the presence of nonlinear stiffness increases the values of U^* for all values of κ in this range. For example, at $\kappa = 8 \times 10{-6}$, there is an increase of $7,679\%$ in U^* when nonlinear stiffness is included. Increasing flutter speed is interesting for aeronautics, because it can indicate that flight speed can be increased.
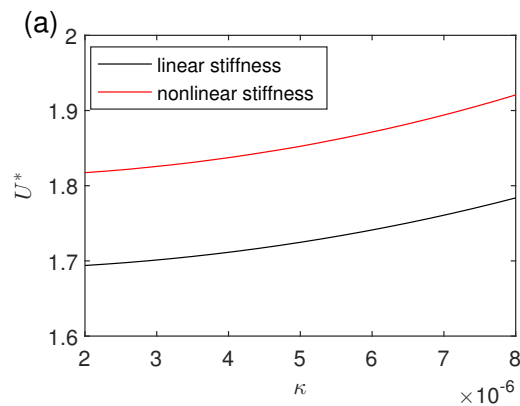
Figure 2. Flutter speed as a function of the electromechanical coupling.

5 Conclusions

In this work we explore the method of multiple scales to analyse energy harvesting in aeroelastic system in flutter condition, the approximated solution for the steady state motion of the system with nonlinear stiffness was calculated through multiple scales. The multiple scales is an interesting method to analyse flutter condition, and, posteriorly, the TET (target energy transfers) at this type of aeroelastic system.

The flutter speed as a function of electromechanical coupling was found by an otimization method (interval halving method). The results indicates that flutter speed increases with electromechanical coupling. Also, the presence of nonlinear stiffness increases the values of flutter speed, which is interesting for aeronautics, because it can indicate that flight speed can be increased.

Autorship statement. The authors hereby confirm that they are the sole liable persons responsible for the authorship of this work, and that all material that has been herein included as part of the present paper is either the property (and authorship) of the authors, or has the permission of the owners to be included here.

References

[1] M. Safaei, H. A. Sodano, and S. R. Anton. A review of energy harvesting using piezoelectric materials: state-of-the-art a decade later (2008–2018). *Smart Materials and Structures*, vol. 28, n. 11, pp. 113001, 2019.

[2] F. I. Petrescu, A. Apicella, R. V. Petrescu, S. Kozaitis, R. Bucinell, R. Aversa, and T. Abu-Lebdeh. Environmental protection through nuclear energy. *American Journal of Applied Sciences*, vol. 13, n. 9, pp. 941–946, 2016.

[3] C. Wei and X. Jing. A comprehensive review on vibration energy harvesting: Modelling and realization. *Renewable and Sustainable Energy Reviews*, vol. 74, pp. 1–18, 2017.

[4] A. Bibo and M. F. Daqaq. Energy harvesting under combined aerodynamic and base excitations. *Journal of sound and vibration*, vol. 332, n. 20, pp. 5086–5102, 2013.

[5] M. G. Kang, W. S. Jung, C. Y. Kang, and S. J. Yoon. Recent progress on pzt based piezoelectric energy harvesting technologies. In *Actuators*, volume 5, pp. 5. Multidisciplinary Digital Publishing Institute, 2016.

[6] Z. Yang, A. Erturk, and J. Zu. On the efficiency of piezoelectric energy harvesters. *Extreme Mechanics Letters*, vol. 15, pp. 26–37, 2017.

[7] C. Marqui Jr, D. Tan, and A. Erturk. On the electrode segmentation for piezoelectric energy harvesting from nonlinear limit cycle oscillations in axial flow. *Journal of Fluids and Structures*, vol. 82, pp. 492–504, 2018.

[8] R. L. Bisplinghoff, H. Ashley, and R. L. Halfman. *Aeroelasticity*, volume 1. Courier Corporation, 2013.

[9] E. Jonsson, C. Riso, C. A. Lupp, C. E. S. Cesnik, J. Martins, and B. I. Epureanu. Flutter and post-flutter constraints in aircraft design optimization. *Progress in Aerospace Sciences*, vol. 109, pp. 100537, 2019.

[10] N. Tsushima and W. Su. Flutter suppression for highly flexible wings using passive and active piezoelectric effects. *Aerospace Science and Technology*, vol. 65, pp. 78–89, 2017.

[11] A. Abdelkefi, A. H. Nayfeh, and M. R. Hajj. Modeling and analysis of piezoaeroelastic energy harvesters. *Nonlinear Dynamics*, vol. 67, n. 2, pp. 925–939, 2012.

[12] A. Triplett and D. D. Quinn. The effect of non-linear piezoelectric coupling on vibration-based energy harvesting. *Journal of Intelligent Material Systems and Structures*, vol. 20, n. 16, pp. 1959–1967, 2009.

[13] V. C. Sousa, T. M. P. Silva, and C. Marqui Jr. Aeroelastic flutter enhancement by exploiting the combined use of shape memory alloys and nonlinear piezoelectric circuits. *Journal of sound and vibration*, vol. 407, pp. 46–62, 2017.

[14] A. H. Nayfeh and D. T. Mook. *Nonlinear oscillations*. John Wiley & Sons, 2008.

[15] H. Liu and X. Gao. Vibration energy harvesting under concurrent base and flow excitations with internal resonance. *Nonlinear Dynamics*, vol. 96, n. 2, pp. 1067–1081, 2019.

[16] A. Bibo, A. H. Alhadidi, and M. F. Daqaq. Exploiting a nonlinear restoring force to improve the performance of flow energy harvesters. *Journal of applied Physics*, vol. 117, n. 4, pp. 045103, 2015.

[17] C. Marqui Jr and A. Erturk. Electroaeroelastic analysis of airfoil-based wind energy harvesting using piezoelectric transduction and electromagnetic induction. *Journal of Intelligent Material Systems and Structures*, vol. 24, pp. 846–854, 2013.

[18] E. H. Dowell, H. C. Curtiss, R. H. Scanlan, and F. Sisto. *A modern course in aeroelasticity*, volume 3. Springer, 1989.